Greve, J., Maestre, M. F., Moise, H., & Hosoda, J. (1978) *Biochemistry 17*, 887–893.
Jensen, D. E., Kelly, R. C., & von Hippel, P. H. (1976) *J. Biol. Chem. 251*, 7215–7228.
Kedinger, C., Brison, O., Perrin, F., & Wilhelm, J. (1978) *J. Virol. 26*, 364–379.
Kitchingman, G. R. (1985) *Virology 146*, 90–101.
Klein, H., Maltzman, W., & Levine, A. J. (1979) *J. Biol. Chem. 254*, 11051–11060.
Klessig, D. F., & Grodzicker, T. (1979) *Cell (Cambridge, Mass.) 17*, 957–966.
Konings, R. N. H., Jansen, J., Cuypers, T., & Schoenmakers, J. G. G. (1973) *J. Virol. 12*, 1466–1472.
Kruijer, W., Van Schaik, F. M. A., & Sussenbach, J. S. (1981) *Nucleic Acids Res. 9*, 4439–4457.
Kruijer, W., Van Schaik, F. M. A., Speyer, J. G., & Sussenbach, J. S. (1983) *Virology 128*, 140–153.
Lindenbaum, J. O., Field, J. & Hurwitz, J. (1986) *J. Biol. Chem. 261*, 10218–10227.
Linnê, T., & Philipson, L. (1980) *Eur. J. Biochem. 103*, 259–270.
Nevins, J. R., & Jensen-Winkler, J. (1980) *Proc. Natl. Acad. Sci. U.S.A. 77*, 1893–1897.
Nicolas, J. C., Ingrand, D., Sarnow, P., & Levine, A. J. (1982) *Virology 122*, 481–485.
Quinn, C. O., & Kitchingman, G. R. (1984) *J. Biol. Chem. 259*, 5003–5009.
Rice, S. A., & Klessig, D. F. (1984) *J. Virol. 49*, 35–49.
Savitsky, A., & Golay, M. J. E. (1964) *Anal. Chem. 36*, 1627–1639.
Schechter, W. M., Davies, W., & Anderson, C. W. (1980) *Biochemistry 19*, 2802–2810.
Scheerhagen, M. A., van Amerongen, H., van Grondelle, R., & Blok, J. (1985a) *FEBS Lett. 179*, 221–224.
Scheerhagen, M. A., Kuil, M. E., van Grondelle, R., & Blok, J. (1985b) *FEBS Lett. 184*, 221–225.
Scheerhagen, M. A., Blok, J. & van Grondelle, R. (1985c) *J. Biomol. Struct. Dyn. 2*, 821–829.
Scheerhagen, M. A., Bokma, J. T., Vlaanderen, C. A., Blok, J., & van Grondelle, R. (1986a) *Biopolymers 25*, 1419–1448.
Scheerhagen, M. A., Vlaanderen, C. A., Blok, J. & van Grondelle, R. (1986b) *J. Biomol. Struct. Dyn. 3*, 887–898.
Sigal, N., Delius, H., Kornberg, T., Gefter, M., & Alberts, B. M. (1972) *Proc. Natl. Acad. Sci. U.S.A. 69*, 3537–3541.
Specter, T. (1978) *Anal. Biochem. 86*, 142–146.
Steinier, J., Termonia, Y., & Deltour, J. (1972) *Anal. Chem. 44*, 1906–1909.
Torbet, J., Gray, D. M., Gray, C. W., Marvin, D. A., & Siegrist, H. (1981) *J. Mol. Biol. 146*, 305–320.
Tsernoglou, D., Tucker, A. D., & van der Vliet, P. C. (1984) *J. Mol. Biol. 172*, 237–239.
Tsernoglou, D., Tsugita, A., Tucker, A. D., & van der Vliet, P. C. (1985) *FEBS Lett. 188*, 248–252.
van der Vliet, P. C., & Levine, A. J. (1973) *Nature (London), New Biol. 246*, 170–174.
van der Vliet, P. C., Levine, A. J., Ensinger, M. J., & Ginsberg, H. S. (1975) *J. Virol. 15*, 348–354.
van der Vliet, P. C., Keegstra, W., & Jansz, H. S. (1978) *Eur. J. Biochem. 86*, 389–398.

NMR–Pseudoenergy Approach to the Solution Structure of Acyl Carrier Protein†

T. A. Holak and J. H. Prestegard*
Department of Chemistry, Yale University, New Haven, Connecticut 06511
J. D. Forman
Department of Molecular Biophysics and Biochemistry, Yale University, New Haven, Connecticut 06511
Received September 10, 1986; Revised Manuscript Received March 5, 1987

ABSTRACT: A method for protein structure determination from two-dimensional NMR cross-relaxation data is presented and explored by using short amino acid segments from acyl carrier protein as a test case. The method is based on a molecular mechanics program and incorporates NMR distance constraints in the form of a pseudoenergy term that accurately reflects the distance-dependent precision of NMR cross-relaxation data. When it is used in an indiscriminant fashion, the method has a tendency to produce structures representing local energy minima near starting structures, rather than structures representing a global energy minimum. However, stepwise inclusion of energy terms, beginning with a function heavily weighted by backbone distance constraints, appears to simplify the potential energy surface to a point where convergence to a common backbone structure from a variety of starting structures is possible. In the case of the segment from residues 3 to 15 in acyl carrier protein, a nearly perfect α-helix is produced starting with a linear chain, an α-helical chain, or a chain having residues with alternating linear and α-helical backbone torsional angles. In the case of the segment from residues 26 to 36 a structure having a right-handed loop is produced.

Through use of high-field proton NMR[1] and two-dimensional acquisition methods, it has recently become possible, without the aid of previous X-ray crystal structures, to attempt structure determinations of proteins in solution (Braun et al., 1981, 1983; Kaptein et al., 1985; Zuiderweg et al., 1985a; Williamson et al., 1985; Braun et al., 1986; Kline et al., 1986). While published attempts appear to be successful in some cases, there is still no universally accepted procedure for

†Supported by a grant from the National Institutes of Health (GM32243) and an instrumentation grant provided through shared instrumentation programs of the National Institute of General Medical Science (GM32243S1) and the Division of Research Resources of the NIH (RR02379).

[1] Abbreviations: ACPSH, acyl carrier protein with the free SH group; 2D NMR, two-dimensional nuclear magnetic resonance; DQF COSY, double quantum filtered two-dimensional J-correlated NMR spectroscopy; NOE, nuclear Overhauser effect; NOESY, two-dimensional NOE spectroscopy.

0006-2960/87/0426-4652$01.50/0

structure determination and there is still some skepticism about the validity of structures produced. It is our intent to evaluate one approach to structure determination, a molecular mechanics–NMR pseudoenergy approach, by examining structures produced for a 13-residue segment at the amino terminus of a small soluble protein, acyl carrier protein (ACPSH).

All NMR-based structure determination methods rest on the presumption that proton–proton cross-relaxation rates can be converted to estimates of interproton distances and that a sufficiently large set of interproton distances will uniquely define a protein structure (Braun et al., 1981, 1983; Havel & Wüthrich, 1985; Brünger et al., 1986; Clore et al., 1986). The methods differ in the particular algorithms used to find a structure and in the ways they attempt to compensate for imprecise or inadequate distance information.

The earliest algorithms are based on the distance geometry method of Kuntz et al. (Kuntz et al., 1979; Havel et al., 1979, 1983) in which upper and lower bounds for interproton distances are defined in boundary matrices, and a search for a structure having a matrix representation between these bounds is executed (Braun et al., 1981, 1983, 1986; Arseniev et al., 1984; Williamson et al., 1985; Kline et al., 1986). New algorithms have improved the speed and the ability of these basic methods to deal with larger structures (Kuntz et al., 1979; Havel & Wüthrich, 1984, 1985; Braun & Gō, 1985), and the methods have been extensively applied (Braun et al., 1981, 1983, 1986; Arseniev et al., 1984; Williamson et al., 1985; Kline et al., 1986). Distance geometry methods, in general, are efficient and nicely allow for the uncertainties in NMR data in that only bounds to distances need to be specified. However, when NMR data alone are inadequate, inclusion of supplementary structural information, such as that based on our knowledge of chemical bonding, can be difficult. Inclusion may be restricted to fixing bond lengths and bond angles, and perhaps including a van der Waals repulsion term.

Molecular mechanics and molecular dynamics programs that use empirical potential energy functions to represent molecular properties would seem to provide an alternate approach. These programs provide an efficient means of including our accumulated knowledge of preferred bond geometries in the calculation of a final structure and allow placement of portions of proteins, side chains for example, in reasonable conformations even when they may not be adequately constrained by NMR data. NMR constraints can be included in the form of an appropriate pseudoenergy function. These constraints are, of course, in no sense real energies, but they can be written in the form of a distance-dependent function that minimizes when a preferred geometry is found, much as the real energy functions representing bonded and nonbonded interactions among atoms. The use of pseudoenergies in either a molecular dynamics approach or a molecular mechanics approach is appealing because it would seem possible to tailor the pseudoenergy function to accurately reflect the precision of NMR distance measurements. It would also seem possible to allow a realistic interplay of NMR and chemical bonding constraints by choice of an appropriate weighting function for the pseudopotential.

Molecular dynamics programs, which are able to explore large allowed regions of conformational space without restriction to a local energy minimum, have been used recently to find a final structure that satisfies both bonding constraints and NMR constraints (Kaptein et al., 1985; Zuiderweg et al., 1985a; Clore et al., 1985, 1986; Brünger et al., 1986). NMR constraints have been included in these programs as pseudopotentials, but it is not clear that they have been optimized to represent precision in NMR data (Kaptein et al., 1985).

Although a number of molecular mechanics programs exist that are capable of dealing with macromolecules, use of these programs for structure determination has been explored less thoroughly. In cases where they have been employed, problems with trapping in local, rather than global, energy minima have restricted their use to either early stages, or final refinement stages of structure searches (Kaptein et al., 1985; Zuiderweg et al., 1985a; Clore et al., 1985). Below we describe an improved pseudoenergy function and test procedures that may allow us to locate global minimum structures from widely different starting structures using a molecular mechanics program.

As a test we will attempt to generate an α-helix believed to be present at residues 3–15 in acyl carrier protein from *Escherichia coli*. ACPSH is a protein of molecular weight 8847 that acts as a carrier of fatty acids during their synthesis by the fatty acid synthetase system (Thompson, 1981; Wakil et al., 1983). We recently reported the complete assignment of backbone proton resonances of this protein and sufficient cross-relaxation data to define general secondary-structure features (Holak & Prestegard, 1986). α-Helices are easily identified by qualitative interpretation of NOE data (Wüthrich et al., 1984). Observation of strong amide–amide and nearly as strong amide–$C^{\alpha}H$ connectivities in 2D NOESY plots for residues adjacent in the sequence, along with weaker connectivities between resonances assigned to $C^{\alpha}H$ and amide protons on residues three and four removed in the sequence, is highly suggestive of an α-helix. This is particularly so when these connectivities occur over a long segment of the structure as in the case of residues 3–15. It is these connectivities we will quantitate, incorporate as pseudoenergies, and use to generate structures from divergent starting points in our initial test. We will subsequently investigate application to a nonhelical segment, residues 26–36.

Methods

Molecular Mechanics Program. In choosing a program in which to incorporate NMR pseudoenergies and test protocols for the determination of structure, one would seek a program with a well-tested molecular mechanics basis, a convenient means of generating starting structures, some flexibility in the way in which various energy contributions are incorporated, and adequate modules for the comparison and output of structures. We have chosen a package introduced by Weiner and Kollman (1981) and brought to its current version by Singh et al. (1984).[2] The program, called AMBER for Assisted Model Building with Energy Refinement, uses an energy function similar to that used by Gelin and Karplus (1979), but the energy functions have been further refined at both the C–H united atom and all-atom levels (Weiner et al., 1984, 1986). This program meets most of the criteria mentioned above.

We have altered the data base slightly to tailor it for use with NMR data and to allow more flexibility in generating starting structures. Amino acid structures may include all atoms, or they may be reduced in complexity by considering all hydrogens on carbons as part of a united atom centered at the carbon but with force field parameters chosen to mimic properties of the entire group. The united atom approach is in many respects ideal for NMR calculations since the precise

[2] AMBER 2.0 (U.C. Singh, P. K. Weiner, D. A. Case, J. Caldwell, and P. A. Kollman, 1985) is a program obtained through a licensing agreement with the Regents of the University of California at San Francisco.

position of protons on side chains is frequently not known because of rapid internal rotations or an inability to make stereospecific assignments. This is a fact that has been recognized for some time. In fact, Wüthrich et al. (1983) have introduced a type of NMR pseudoatom for distance geometry calculations to avoid these ambiguities. United atoms are not, however, desirable in all cases. We do, for example, often know precise positions for α protons, amide protons, β protons in valine, and β protons in isoleucine. A hybrid amino acid type was therefore constructed that contained mostly united atoms in place of hydrogen-bearing carbons but explicit hydrogens in cases where precise NMR distance information may be expected. Charges on atoms were adjusted to maintain appropriate net charges for each new amino acid, and force constants for the new types of bonds were added to the parameter files drawing on analogies with values already appearing.

The existing AMBER data base for proteins allows the linking of amino acids into a low-energy, nearly linear conformation, based on input of sequence information. It also allows alteration of the initial conformation by overlaying portions of existing X-ray structures. However, for cases where X-ray structures do not exist, it is useful to have another means of generating alternate starting structures. The amino acid data base was therefore expanded to include a set of amino acids having α-helical conformations. Any mixture of α-helical and linear amino acid types could be linked, in principle allowing 2^{13} starting points for the segment to be studied here.

Pseudoenergy Function. The pseudoenergy function was chosen on the basis of computational simplicity and ability to represent precision in NMR data. Ideally cross peaks in short mixing time 2D NOESY data sets have intensities, and signal to noise ratios, proportional to $1/r_{0ij}^6$, where r_{0ij} is the experimental interproton distance in angstroms (Wagner & Wüthrich, 1979; Anil Kumar et al., 1981; Dobson et al., 1982; Keepers & James, 1984; Clore & Gronenborn, 1985). In actual fact, this simple proportionality can be complicated by anisotropic and internal motions. Recent estimates, however, suggest that neglect of these complications leads to only minor distance errors (Olejniczak et al., 1984a). The pseudoenergy function should therefore have a minimum at r_{0ij} and have a derivative with respect to $(r_{ij} - r_{0ij})$ proportional to $1/r_{ij}^7$, where r_{ij} is the corresponding interproton distance in angstroms in any trial structure. We have experimented with a function that satisfies exactly these criteria using a global search program in our work on carbohydrate structure (Scarsdale et al., 1986). The function unfortunately is not smooth at $r_{ij} = r_{0ij}$, making it inappropriate for most energy minimization programs. We use instead the function (Scarsdale et al., 1987)

$$E_{\text{pseudo}} = W(729\ \text{Å}^6)[(1/r_{ij}^3 - 1/r_{0ij}^3)^2 - 1/r_{0ij}^6] \quad (1)$$

W is a weighting factor (kcal/mol) chosen to allow the appropriate interplay of distance and normal bonding constraints. In the final stages of our calculations we choose it so that NMR constraints observed with high precision, for example, those at 3 Å, will dominate bonding contributions not well represented in the calculations, for example those from hydrogen bonds or solvation. The function does have a minimum at r_{0ij}, with depth proportional to $1/r_{0ij}^6$, and it has an appropriate distance dependence at short r_{ij} where NMR data would be most valid. The function makes a somewhat larger energy contribution than it should at large r_{ij}. This, however, appears to be an advantage in providing reasonably rapid convergence.

Aside from providing a reasonable approximation to precision of NMR data, the function offers some other advantages over the simple harmonic functions that have been used in other applications (Kaptein et al., 1985; Zuiderweg et al., 1985a; Clore et al., 1985, 1986; Brünger et al., 1986). First, it automatically allows shorter constraints to dominate convergence in the early stages of the calculations. This may be advantageous on the basis of recent observations in molecular dynamics and distance geometry calculations suggesting that early inclusion of long-range constraints can result in premature folding of chains in a way that prevents formation of proper secondary structure (Brünger et al., 1986; Clore et al., 1986; Braun & Gō, 1985). Second, the steep r_{0ij} dependence makes pseudoenergy contributions approach zero for long interproton distances. This allows incorporation of nonobserved connectivities in the NOESY spectra by setting r_{0ij} to a distance at which connectivities would be lost in the noise, in our case approximately 5 Å. These additions would contribute almost nothing to constraint energies as long as the corresponding interproton distances in the structures generated were more than 5 Å, but it would effectively exclude conformations in which the distances were so short that connectivities should be observed. We have taken advantage of this in only a few cases where the absence of the expected connectivities could be determined unambiguously. For example, the distances G12HA1–L15NH, G12HA2–L15NH, and R6HA–K10NH were set to ca. 5 Å (Table I) because of the absence of the $C^{\alpha}H(i)$–$NH(i + 3, 4)$ connectivities.

Distance Determination. The interproton distances, r_{0ij}, to be used in the pseudoenergy function described above were obtained from two-dimensional cross-relaxation experiments. The data were acquired on a 10 mM sample of ACPSH at pH 5.3 in 55 mM KH_2PO_4 with use of a pulse sequence designed to yield a phase-sensitive NOESY spectrum (States et al., 1982). The spectra were acquired with 2K complex points in the 5-kHz f_2 frequency domain and with 317 (80-ms mixing time) and 550 (150-ms mixing time) points in the 5-kHz f_1 frequency domain. In each case the time domain data matrix was expanded to 2K in t_1 by zero filling.

The data sets were processed with two different window functions. In one case Lorentzian-to-Gaussian transformation (GM) was used in both dimensions with a line-broadening factor equal to −2 and a Gaussian decay constant set to 0.3 times the acquisition time. In the other case, the t_2 domain was multiplied by the same GM function, whereas the t_1 dimension was processed with a sine-bell function shifted by 24° and extended to 317 data points. Gaussian apodization is preferred to exponential multiplication in measurements of peaks areas in spectra of macromolecules because of the improved delineation of resonances near the base line (Weiss et al., 1987). It is also useful in eliminating some of the t_1 noise and dispersion components of slightly incorrectly phased peaks (Williamson et al., 1985; Ferrige & Lindon, 1978). The use of a sine-bell function in the t_1 dimension further eliminates t_1 noise but can introduce systematic errors in intensity measurements when peaks of different width are involved. Figure 1 shows a representative portion of the 80-ms data set processed with the GM sine-bell functions. However, the set processed with the Gaussian functions was used exclusively in all calculations.

In these data sets a cross peak at a position corresponding to the chemical shift of the proton donating magnetization in the f_1 dimension and the chemical shift of the proton receiving magnetization in the f_2 dimension will grow and then decay as a function of the mixing time. While the expected time course of growth and decay can be accurately described throughout the relaxation process even for very complex spin

Table I

connectivity[a]	dist[b]	A[c]	M[c]	L1[c]	L2[c]	wt[d]
I3NH–E4NH	2.8	−0.0	−0.0	−0.0	−0.0	30
E4NH–E5NH	2.8	−0.0	−0.0	−0.0	−0.0	30
E5NH–R6NH	2.7	0.0	0.0	0.0	0.1	30
R6NH–V7NH	2.8	−0.0	−0.0	−0.0	0.1	30
V7NH–K8NH	2.9	−0.0	−0.0	−0.0	−0.1	30
K8NH–K9NH	2.8	0.0	−0.0	0.0	0.6	15
K9NH–I10NH	3.2	−0.1	−0.1	−0.1	−0.1	30
I10NH–I11NH	3.1	−0.1	−0.1	−0.1	−0.0	30
I11NH–G12NH	2.9	−0.0	−0.0	−0.1	−0.1	30
G12NH–E13NH	3.0	−0.1	−0.1	−0.1	−0.1	30
E13NH–Q14NH	2.7	0.0	−0.0	−0.0	0.0	30
Q14NH–L15NH	3.1	−0.1	0.1	−0.1	−0.0	30
I3HA–E4NH	3.9	−0.2	−0.2	−0.2	−0.2	30
E4HA–E5NH	3.0	0.6	0.6	0.5	−0.0	15
E5HA–R6NH	3.6	−0.1	−0.1	−0.1	−0.2	30
R6HA–V7NH	3.4	0.1	0.1	−0.1	0.0	30
V7HA–K8NH	3.7	−0.1	−0.1	−0.1	0.1	30
K8HA–K9NH	3.0	0.5	0.5	0.5	0.3	30
K9HA–I10NH	3.2	0.3	0.4	0.3	−0.3	30
I10HA–I11NH	3.3	0.3	0.3	0.3	−0.0	30
I11HA–G12NH	3.0	0.5	0.5	0.5	0.6	30
G12HA1–E13NH	3.0	−0.1	−0.1	−0.1	0.3	30
G12HA2–E13NH	3.0	0.4	0.5	0.4	−0.1	30
Q14HA–L15NH	3.0	0.5	−0.1	0.5	0.1	30
E4HA–V7NH	3.3	0.0	0.0	0.1	1.1	30
E5HA–K8NH	3.1	0.1	0.1	0.1	0.0	30
R6HA–K9NH	3.4	0.1	0.1	0.1	5.9	15
V7HA–I10NH	3.5	−0.1	−0.1	−0.1	3.1	30
K8HA–I11NH	3.0	0.0	0.0	0.0	0.1	30
K9HA–G12NH	3.4	0.2	0.2	0.2	1.6	30
I10HA–E13NH	3.5	−0.1	−0.2	−0.0	4.4	30
I11HA–Q14NH	3.1	0.0	0.0	−0.0	0.0	30
G12HA1–L15NH	5.0	0.3	2.3	0.5	1.8	8
G12HA2–L15NH	5.0	−0.9	1.8	−0.7	2.4	8
I3HA–V7NH	4.0	−0.0	0.1	0.1	2.3	30
E4HA–K8NH	4.0	0.0	−0.1	−0.1	0.7	30
E5HA–K9NH	4.0	0.1	0.1	0.1	1.6	15
K6HA–I10NH	5.5	−1.2	−1.1	−1.3	4.9	15
V7HA–I11NH	3.7	0.6	0.6	0.4	2.7	30
K8HA–G12NH	3.8	0.1	0.1	0.1	1.7	30
I10HA–Q14NH	4.1	−0.0	0.3	0.1	3.6	30
I11HA–L15NH	3.7	0.1	1.4	−0.0	1.7	30
I3CG2–V7NH	5.3	0.0	0.0	0.1	3.3	8
I3HB–E4NH	2.7	−0.0	−0.0	−0.0	−0.0	30
V7HB–K8NH	2.6	0.0	0.0	0.0	−0.0	30
K9CB–I10NH	3.0	−0.1	−0.1	−0.1	1.1	15
I10HB–I11NH	3.0	−0.1	−0.1	−0.1	0.4	30
I11HB–G12NH	2.6	0.0	0.0	0.0	−0.0	30
E13CB–Q14NH	3.2	−0.2	0.1	−0.2	0.7	8
Q14CB–L15NH	3.0	−0.0	0.9	0.0	0.7	15
I3CG2–E4NH	4.1	−0.4	−0.4	−0.4	0.3	15
V7CG1–K8NH[e]	4.2	−0.5	−0.5	−0.4	−0.6	15
V7CG2–K8NH[e]	4.7	−0.2	−0.2	−0.2	−0.2	15
I10CG2–I11NH	4.0	0.2	0.2	0.2	−0.1	15
I11CG2–G12NH	4.0	−0.4	−0.4	−0.0	0.3	15
I3NH–I3HA	3.1	−0.1	−0.1	−0.1	−0.1	30
E4NH–E4HA	2.9	−0.0	−0.0	−0.0	0.0	30
E5NH–E5HA	2.3	0.3	0.3	0.3	0.2	10
R6NH–R6HA	2.8	0.0	0.0	0.0	−0.2	30
V7NH–V7HA	2.9	−0.0	−0.0	−0.0	0.0	30
K8NH–K8HA	2.9	−0.0	−0.0	−0.0	0.0	30
K9NH–K9HA	2.5	0.1	0.1	0.1	−0.0	30
I10NH–I10HA	2.9	−0.1	−0.1	−0.1	−0.2	30
I11NH–I11HA	2.7	0.0	0.0	0.0	0.1	30
G12NH–G12HA1	2.4	−0.0	0.0	−0.0	0.2	10
G12NH–G12HA2	2.7	0.0	0.1	0.0	−0.2	10
E13NH–E13HA	2.7	0.1	0.1	0.1	−0.1	30
Q14NH–Q14HA	2.7	0.0	−0.1	−0.0	0.0	30
L15NH–L15HA	2.6	0.0	0.0	0.0	0.0	30
I3NH–I3HB	2.5	0.0	0.0	0.0	0.0	15
E4NH–E4CB	2.5	0.0	0.0	−0.0	0.1	8
R6NH–R6CB	2.7	−0.1	−0.1	−0.1	0.6	8
V7NH–V7HB	2.4	0.0	0.0	0.0	0.0	15
K8NH–K8CB	2.8	−0.2	−0.2	−0.2	−0.2	8
K9NH–K9CB	2.5	−0.0	−0.0	−0.0	0.5	15
I10NH–I10HB	2.6	0.0	0.0	−0.0	0.2	15
I11NH–I11HB	2.5	−0.0	−0.0	0.0	0.1	15
E13NH–E13CB	2.9	−0.2	−0.3	−0.2	0.5	8
Q14NH–Q14CB	2.4	0.0	0.4	0.0	0.0	8
L15NH–L15CB	2.4	0.0	0.0	0.0	0.0	15
I3NH–I3CG1	3.5	−0.2	−0.2	−0.2	0.6	15
I3NH–I3CD1	4.9	−0.6	−0.5	−0.5	0.2	15
I3NH–I3CG2	4.4	−0.2	−0.2	−0.2	−0.6	15
V7NH–V7CG1[e]	4.2	−0.1	−0.1	−0.1	−0.0	15
V7NH–V7CG2[e]	3.5	−0.4	−0.4	−0.4	−0.1	15
I10NH–I10CG2	4.3	−0.2	−0.2	−0.2	0.2	15
I11NH–I11CG2	3.9	0.2	0.2	0.1	−0.0	15

[a] The amino acid residues are identified by the one-letter symbol followed by a number indicating the position in the amino acid sequence. NH stands for amide proton; HA for $C^{\alpha}H$ proton; HB for $C^{\beta}H$ proton; CB, CG, and CD indicate united atoms that substitute for two or three protons in $C^{\beta}H$, $C^{\gamma}H$, and $C^{\delta}H$ methylene/methyl protons, respectively (see text). [b] Distance constraints (Å) estimated from the relative intensities of cross peaks in the NOESY spectrum (mixing time, 80 ms) as described in the text. Additional constraints used in all the steps of the calculations were the (C=O oxygen(i))–(NH proton (i + 1)) distances set to 3.13 Å (weights, 30 kcal/mol). [c] Starting structures were α-helix (A), an extended β-strand (L), and an a mixed conformation (M) in which residues, starting with amino end, alternate their conformation between α-helical and linear extended structures. Differences between calculated distances of final structures and distance constraints (column 2) are given in columns 3–6. [d] Final pseudoenergy weighting factor (kcal/mol). [e] The methyl resonances $C^{\gamma 1}H_3$ and $C^{\gamma 2}H_3$ of Val-7 were assigned stereospecifically using the method of Zuiderweg et al. (1985). The $J_{\alpha\beta}$ coupling constant was measured from the pure absorption DQF COSY spectrum (data not shown) and was equal to 11 Hz. Note that the designation of methyl γ^1 and γ^2 in the Zuiderweg et al. paper should be interchanged in order to conform to the IUPAC–IUB convention (IUPAC–IUB Commission on Biochemical Nomenclature, 1970) used in the AMBER program.

systems (Kay et al., 1986a), it is most easily analyzed in the short mixing time limit (Wagner & Wüthrich, 1979; Anil Kumar et al., 1981; Braun et al., 1981; Dobson et al., 1982; Olejniczak et al., 1984b). Here intensity is proportional to the inverse sixth power of the interproton distance, with the proportionality constant containing factors such as the number of donating and receiving spins and a spectral density function dependent on the effective correlation time modulating the interaction.

In our studies, two mixing times were used so that data in the two sets could be compared to assure that data from the shorter mixing time was in a portion of the time curve where cross peaks grow in a nearly linear fashion. Only data from the shorter mixing time set (80 ms) were used in the final calculations. The proportionality constant mentioned above was evaluated from intensities for cross peaks between protons at known distances. Since we know the 3–15 segment to be in a near α-helical conformation, we chose the average intensities of peaks connecting the $C^{\alpha}H(i)$–NH(i) and NH(i)–NH(i + 1) protons to evaluate the constant. In a perfect α-helix these protons are separated by r_{0kl} = 2.7 and 2.8 Å, respectively. All other distances were calculated from eq 2 in which $I_{kl}r_{0kl}^6$ is the average proportionality constant and I_{ij} is the intensity of the cross peak of interest.

$$r_{0ij} = [(I_{kl}r_{0kl}^6)/I_{ij}]^{1/6} \quad (2)$$

The correctness of the calibration was checked for pairs of protons whose interproton distance is fixed by bonding. The

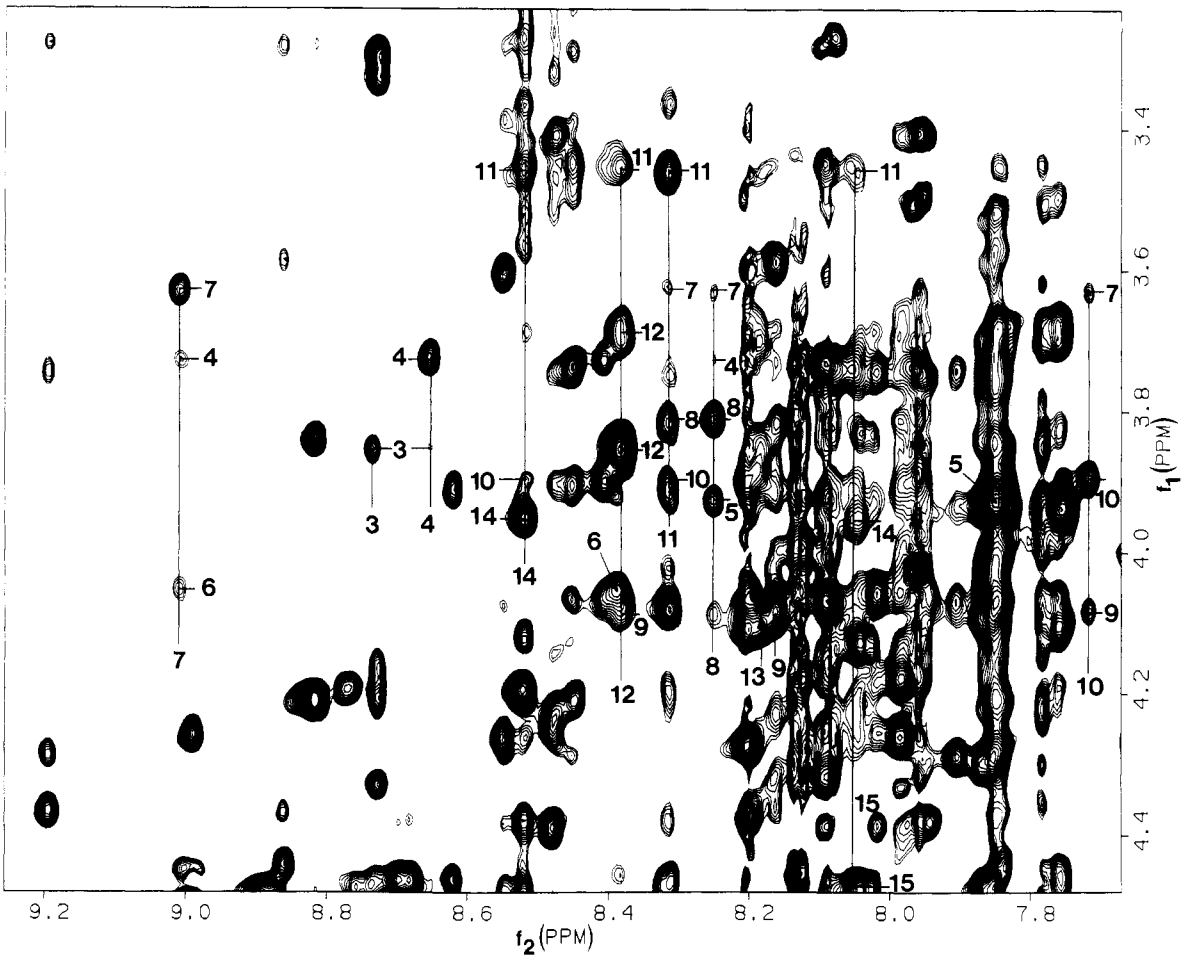

FIGURE 1: Section of a pure absorption 490-MHz ^{1}H NOESY spectrum of ACPSH, pH 5.3, mixing time 80 ms, containing the amide–C$^\alpha$H connectivities for residues 3–15. Peaks labeled include C$^\alpha$H(i)–NH(i + 1), C$^\alpha$H(i)–NH(i + 3), and C$^\alpha$H(i)–NH(i + 4) interrresidue NOEs and C$^\alpha$H(i)–NH(i) intraresidue NOEs. Vertical lines are labeled at the bottom according to their amide resonance positions in the f_2 dimension. Because of spectral overlap, for residues Arg-6, Lys-9, Glu-13, and Leu-15, only the C$^\alpha$H(i)–NH(i) cross peaks are marked.

geminal C$^\alpha$H$_2$ protons of glycines were used for this purpose. In ACP, NOE cross peaks for two out of four glycines show first-order behavior (Kay et al., 1986b) and have easily interpretable intensities (Gly-74, Gly-12). From these intensities and eq 2, the calculated distance H$^\alpha$1–H$^\alpha$2 is 1.84 Å, in very good agreement with the theoretical distance of 1.78 Å.

Intensities used in calculations were obtained from volume integrals. The volume integrals consisted of a sum over all data points within a rectangular base plane defined by selecting corner points displaced vertically and horizontally from the peak center by distances at least 3 times the peak width. When spectral overlap prevented defining a suitable full base plane, either we defined a plane encompassing the better resolved half of a cross-peak with an edge bisecting the peak and multiplied the volume by 2 or we measured a total volume for a selected region and subtracted integrals of the peaks for which it was possible to define base-plane limits.

Even where accurate intensities can be measured, straightforward interpretation in terms of cross-relaxation between a pair of protons rigidly fixed in the protein structure is not always possible. Resonances from the protons on methyls and many methylenes, for example, are not resolved. Even in cases where they are resolved, stereospecific assignments are often not possible. These are the cases where use of united atoms is advantageous. Their use requires the formulation of some rules for the conversion of intensity to distances between a proton and united atom center. These rules are most easily devised for interactions between protons on groups far removed in the protein sequence. Here distances tend to be long and effects of specific group geometries minimal. Consider first the case of a methyl group. Methyls rotate very rapidly under almost all circumstances. Since contributions to cross-relaxation at short times in large molecules are dominated by zero frequency components of the spectral density function, these rapid motions contribute little directly to relaxation but do have an effect by averaging the interaction Hamiltonian. The net effect of this averaging is to make the methyl group appear equivalent to three independent protons located in the plane of the methyl protons at a point on a projection of the heavy atom bond to the methyl group. The distance between this point and a proton yielding a cross peak can be calculated by dividing the observed cross peak intensity by 3 before using eq 2. The distance calculated must then be changed to that between the proton and the united atom center before use in eq 1. This correction depends on methyl group orientation. For a proton at a large distance on the projection of the methyl group symmetry axis it would be +0.33 Å. For a proton in the plane of the methyl protons no correction would be required. Expecting remote contacts to occur most frequently from a point in the direction of the extended side chain, we added 0.33 Å to the distance.

For a methylene group motions are likely to be slower. Consider the case in which interconversion among conformers requires much more time than the time for protein tumbling, $\sim 10^{-9}$ s, and much less time than the time for cross relaxation, $\sim 10^{-1}$ s. Within this rather broad range of time scales, cross peaks seen are the weighted average of cross peaks that would be produced in any one conformer. Because the distance

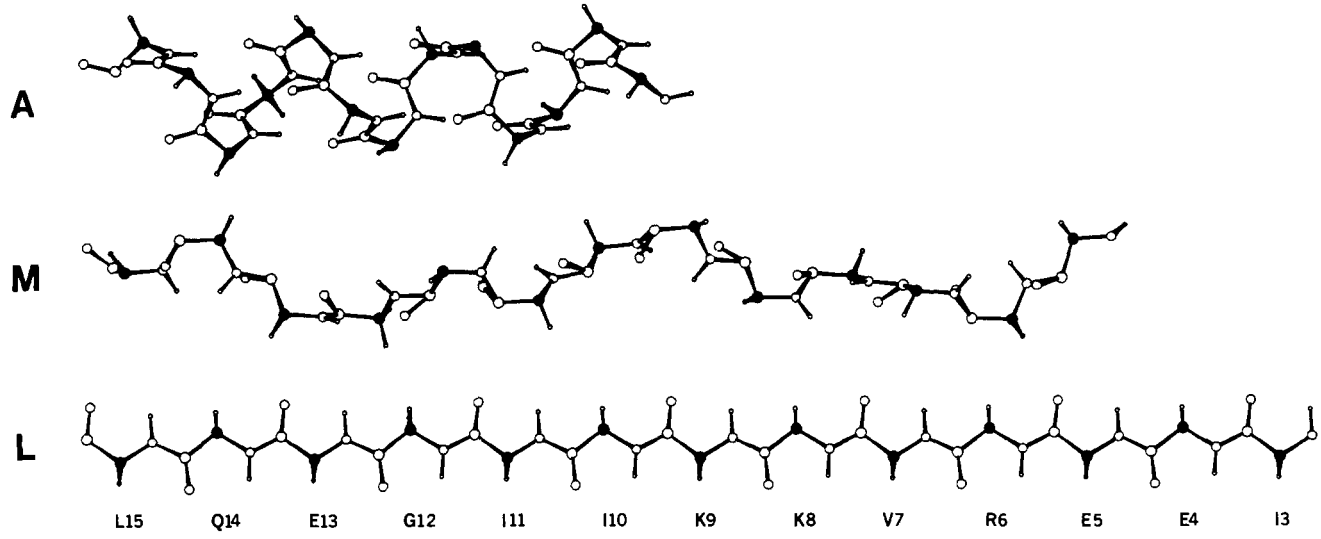

FIGURE 2: Initial structures used in the calculations. Only backbone C^{α} (filled circles), NH, C=O, and $C^{\alpha}H$ atoms are shown.

dependence of cross relaxation is so steep, we will assume that cross relaxation only to the closest proton in each conformer contributes to the cross peak. If we further assume that closest approach is likely to be along the C–H bond, the position of the united atom can be calculated by adding intensities in cross peaks to both methylene protons, calculating a distance from eq 2 assuming only one proton contributes and adding 1.0 Å to get the distance to the united atom. While there are a number of assumptions in this calculation, comparison to calculations for speciic geometries, such as a proton located on the plane of the methylene group, 3.0 Å from each proton and on the side away from the methylene carbon, shows errors in estimated distance to be less than 0.3 Å.

While the above rules prove to be adequate for many situations, there are situations where specific geometries need to be taken into account. Amide proton to β proton distances within the same or adjacent residues, for example, need to be treated differently. Because of the position of the amide proton on the backbone and the tendency of the side chains to extend outward, the closer of the two β-methylene protons is at a distance nearly equal to the amide proton–C^{β}-united atom distance in commonly observed peptide conformations such as the α-helix. Because of this, we have chosen to make no corrections to intraresidue and interresidue i to $i + 1$ connectivities between β-methylene and amide protons when we are working with a suspected α-helix. Similar connectivity-specific corrections have been made by Wüthrich et al. (1983) and Clore et al. (1985) in their treatment of NMR pseudoatoms.

Results and Discussion

Having defined an appropriate pseudoenergy function and some simple rules for the conversion of cross-relaxation data into interproton and proton–united atom distances, we undertook testing of various protocols for structure determination on a segment of reasonably well-defined structure. We reduced data for the 3–15 segment of ACPSH to distance constraints. These constraints are listed in Table I. These constraints were incorporated into our conformational calculations as pseudoenergies using the energy weightings listed in the last column of Table I. The weighting constants are not all equal because there are experimental uncertainties affecting data other than statistical noise and the $1/r^6$ dependence of cross relaxation. Most side-chain proton–amide proton constraints were for example given half the weighting of the backbone proton–amide proton constraints because of uncertainties associated with the use of united atoms. In a few instances other weightings were given because of spectral overlap or other uncertainties.

The three starting structures selected for our calculations are shown in Figure 2. These include an α-helix (A), which we expect to be rather close to the final structure, a linear peptide (L), which should be very far from the final structure, and a hypothetical structure (M), having residues that alternate α-helical and linear conformations for ϕ and ψ torsion angles. That these be energetically reasonable starting points is not required. The latter structure may in fact be rather high in energy.

After starting structures were prepared jobs were submitted for energy minimization on a VAX 11/750. Except in cases where unusually high energies resulted because of unreasonable starting or intermediate structures, a conjugate gradient minimizer was used. Starting step sizes of 0.1 Å were selected, and convergence criteria were set to energy changes of 1×10^{-6} kcal/mol or to the magnitude of the norm of the gradient of 0.1. A rather high dielectric constant (100) was selected to minimize an observed tendency for ion pairs to form. The particular protein segment we chose has a high proportion of charged residues, three negative and three positive. Electrostatic interactions are rather long range and could well dominate the folding process. Since a segment removed from a whole protein may not even contain all the residues required for proper pairing of ions, we felt it best to minimize the effect of these interactions.

Our initial attempts at finding minimum energy structures from each starting point involved a straightforward inclusion of all energy terms using, at first, a high weight for distance constraint energies (10 times larger than those given in the last column of Table I) and then a weight felt to give a suitable mix of real and pseudoenergies ($\sim$15–30 kcal/mol; last column, Table I). Starting with an α-helix resulted in a structure satisfying all distance constraints to within experimental error and a real energy, which refers to the difference between the total energy and the pseudoenergy, of −30 kcal/mol. This is only 17 kcal/mol higher in energy than an α-helix optimized without NMR constraints. This is clearly a viable structure. However, starting with either a mixed conformation (M) or linear conformation (L) and following a similar protocol resulted in structures less compatible with observation. Both showed distance deviations exceeding 1 Å for several proton pairs that give strong, well-defined NOEs. The real energy

associated with the final conformers was also considerably higher than that for the structure produced from an α-helix start. The increased energy is likely the result of interplay of NMR constraints and molecular constraints, neither of which is entirely satisfied in the final structures. The geometries, while having some backbone portions in a helical structure, were observed to maintain some aspects of their starting structures. These results are not unlike the results of other investigators, which have indicated that straightforward application of energy minimization methods is highly susceptible to trapping in local energy minima (Kaptein et al., 1985; Clore et al., 1985).

It seems likely that the tendency to be trapped in local minima should decrease as one simplifies the potential energy surface. We can do this, at least in the early stages of calculation, by minimizing the number of contributions to the energy function. We experimented with several protocols for limiting the number of energy terms at various stages of the calculation. The results of our most successful protocol are summarized in columns labeled A, M, and L1 in Table I. To produce these, we initiated calculations starting from the three starting points, α-helix (A), mixed chain (M), and linear chain (L), having only distance constraints, bond energies, and bond angle energies present. This produces a freely rotating chain of residues that can move without the constraints of nonbonding repulsions and electrostatic interactions. We also eliminated NMR constraints that provide redundant backbone conformational data or dictate side-chain conformations. In particular we removed the constraints involving β and γ protons, and all intraresidue connectivities. Those constraints retained were weighted heavily as before. After converging, 1–4 nonbonding and dihedral energies were added, and after 100 cycles, all other energy contributions, both those molecular in origin and those from additional NMR constraints, were added. After convergence, the distance constraint weightings were relaxed to ~15–30 kcal/mol and a final structure was obtained.

Note that all three structures show excellent agreement with experimental distance constraints. These errors are of order 0.1 Å for distances of 3 Å. They may increase to 0.5 Å or more for larger distances because of the way the cross-relaxation function propagates errors. The total energies for the A, M, and L1 structures were −2499, −2459, and −2469 kcal/mol, and the real energy contributions were −30, −21, and −37 kcal/mol, respectively. Both the total energies and the real energies indicate that the structures are superior to those produced under less successful protocols such as that to be described below (cf. L2 in Table I; −2381 and +70 kcal/mol, respectively). Examination of localized contributions to the real energy suggests that most differences between the three structures result from differences in side-chain conformation. These portions of the molecule were relatively unconstrained, and it is not surprising that they did not reach the same conformations. The similarity of backbone conformation in the three structures is confirmed in the plots shown in Figure 3. Residues 3–13 are almost exactly superimposable. There are some deviations at the segment ends that might be anticipated because of the smaller numbers of distance constraints.

Some minor problems arose in that in two cases chirality of a side-chain carbon inverted. This results when rather high nonbonded and distance constraint energies can overcome energies associated with distortion of bond angles. We found that the problem only occurs with the generation of high-energy intermediate structures and the use of large (~150–300 kcal/mol constraint energies). However, these problems were not encountered for the structures presented in Table I. Also note that despite general agreement of distances in final structures with those experimentally determined, there are some systematic deviations. All calculated distances between $C^{\alpha}H(i)$ protons and amide protons on $i + 1$, $i + 3$, or $i + 4$ residues tend to be too long. It is possible that this is a result of some residual motion in the protein. Any conformational averaging except very rapid motion will tend to accentuate short-distance conformers because of the $1/r_{0ij}^6$ dependence. It would be possible to use slightly different proportionality constants for extracting distances from different types of sequential connectivities. This has been done by other authors (Kline et al., 1986). Also note that distances to methyl groups tend to be too short, suggesting that correcting the distance by an amount smaller than 0.33 Å would have been a better choice. Aside from these problems the protocol outlined above seems very encouraging.

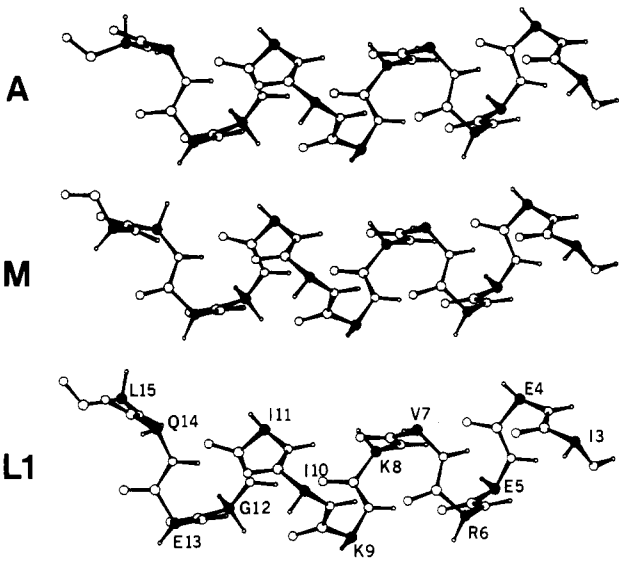

FIGURE 3: Best final structures obtained from the starting structures of Figure 2.

We should point out that the protocol is not infallible. The potential energy surfaces have been simplified, not reduced to a surface with a single extremum. Even seemingly minor modifications of protocol can lead to minimization along an alternate pathway and demonstration that other minima exist. The results of starting from a linear chain and following a protocol identical with that outlined above, except that all NMR constraints, rather than a minimal number, were employed in the first step, are presented in Table I in the column labeled L2. It is clear that the structure does not agree with experiment given the number of distance deviations beyond experimental error. Several connectivities involving residues 9–11 are clearly unacceptable. K8NH–K9NH is 3.4 Å instead of 2.8 Å; V7NH–I10NH is 6.6 Å rather than 3.5 Å; I10HA–E13NH is 7.9 Å rather than 3.5 Å. Also the real energy of the final structure is high, +70 kcal/mol, as opposed to −37 kcal/mol for the conformer represented by the column labeled L1. Other attempts, like ones with the inclusion of all energy terms but with only the NH–NH and NH–$C^{\alpha}H$ interresidue constraints retained in the first stage of the calculations, produced structures with similarly large residual distance violations.

One positive aspect of the calculations, even when local minimum traps are encountered, is that they are easily identified on the basis of distance deviations. These deviations appear at the first stage of minimization, which requires

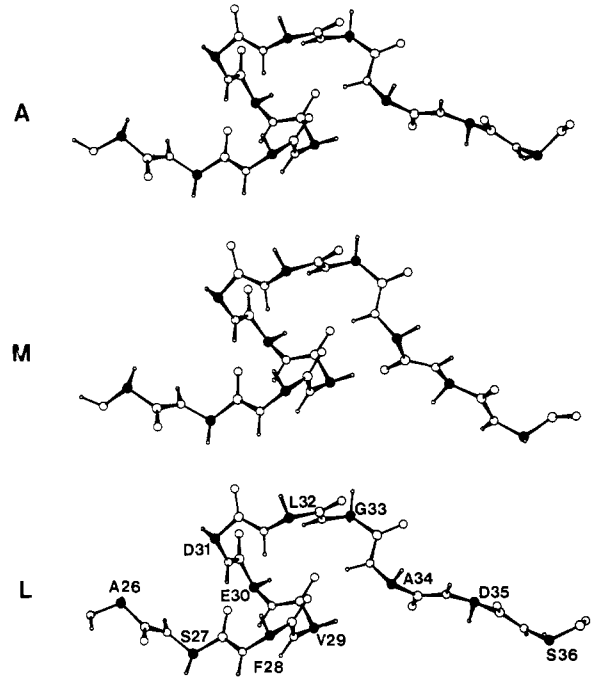

FIGURE 4: Best final structures obtained from the α-helical (A), mixed (M), and linear (L) initial structures for residue segment 26–36 of ACP.

relatively little computer time. Based on inspection of deviations it may even be possible to add some logic in choosing better starting points. In the case described above, for example, one would try torsional angles appropriate for an α-helix for residues 9–11 rather than the angles appropriate for a linear chain.

Because an α-helix is a rather unique structural form, we felt it important to apply our most successful protocol to a segment of ACP having a less easily recognized secondary structure. The stretch of ACP from residues Ala-26 to Ser-36 was selected. This stretch is distinguished by a short contact between NH of Ala-34 and C$^{\alpha}$H of Val-29 and a particularly large number of medium range NOEs to define secondary structure. Patterns in the occurrence of medium-range NOEs can be characteristic of secondary structural elements other than α-helices (Wüthrich et al., 1984; Wagner et al., 1986). Perfect turns types I and II, for example, give rise to characteristic connectivities C$^{\alpha}$H(i)–NH(i + 2) and NH(i)–NH(i + 2). The NOE data for segment 26–36 were checked for all contacts C$^{\alpha}$H(i)–NH(i + 2), C$^{\alpha}$H(i)–NH(i + 3), C$^{\alpha}$H(i)–NH(i + 4), and NH(i)–NH(i + 2). A few were found and are included in Table II, but in no case do they correspond to the precise set expected for a well-characterized secondary-structure element.

The procedure used for calculation of the final structures was the same as that used for the α-helical segment, except that, in the absence of known helical geometry, pseudoatom distance corrections were used for the interresidue connectivities to C$^{\beta}$ atoms. Also, only after initial convergence were constraints for nonobserved NOEs (5 Å) added for proton pairs having close contacts. As can be seen from Figure 4, the three structures produced from linear, α-helical, and mixed starting points are very similar. The linear start produced the final structure without the inclusion of constraints for unobserved NH–NH connectivities. However, both mixed (M) and α-helical (A) starts initially produced a structure containing a *cis*-amide bond between Leu-32 and Gly-33. When unobserved NH–NH constraints 27–28, 34–35, and 35–36 were set to 4.6 Å, the maximum value for the NH–NH distance between sequentially neighboring residues, and given the weight of 300 kcal/mol, convergence to the structures in Figure 4 was produced.

Table II

connectivity[a]	dist[b]	A[c]	M[c]	L[c]	wt[d]
A26NH-S27NH[e]	3.7	0.5	0.5	0.3	30
S27NH-F28NH	4.6	0.0	0.0	0.1	20[f]
F28NH-V29NH	2.9	0.0	0.0	0.0	30
V29NH-E30NH	2.7	0.0	0.0	0.0	30
E30NH-D31NH	2.7	0.1	0.0	0.1	30
D31NH-L32NH	2.5	0.0	0.0	0.0	30
L32NH-G33NH	2.8	−0.0	−0.0	−0.0	20
G33NH-A34NH	2.8	0.1	0.0	0.0	30
A34NH-D35NH	4.6	0.1	−0.1	0.1	30[f]
D35NH-S36NH	4.6	−0.2	−0.2	−0.1	30[f]
A26HA-S27NH	2.1	0.0	0.0	0.0	30
S27HA-F28NH	2.5	−0.1	−0.1	−0.1	10
F28HA-V29NH	3.5	0.0	0.0	0.0	20
V29HA-E30NH	3.6	0.1	0.1	0.1	20
E30HA-D31NH	3.2	0.5	0.5	0.4	8
D31HA-L32NH	3.1	0.3	0.3	0.3	30
L32HA-G33NH	4.3	−0.7	−0.8	−0.8	20
G33HA1-A34NH	3.3	0.1	0.2	0.2	10
G33HA2-A34NH	3.3	−0.3	−0.3	−0.3	10
A34HA-D35NH	2.2	0.0	0.0	0.0	30
D35HA-S36NH	2.6	−0.0	−0.0	−0.0	30
S27NH-D31NH	3.2	0.0	0.0	0.0	30
V29NH-D31NH	4.2	−0.1	−0.1	−0.2	10
D31NH-G33NH	4.3	−0.1	−0.0	−0.2	15
L32NH-A34NH	4.2	−0.4	−0.2	−0.3	15
D31HA-G33NH	4.3	0.1	0.1	0.1	15
S27HA-D31NH	4.3	0.5	0.5	0.4	15
F28HA-L32NH	3.5	0.0	−0.0	−0.0	30
V29HA-G33NH	4.3	0.1	0.4	0.1	15
V29HA-A34NH	2.3	−0.0	−0.0	−0.0	30
S27HN-D31HA	4.2	0.3	0.3	0.1	15
S27NH-D31CB	3.7	−0.0	−0.1	−0.0	20
V29NH-A34CB	4.2	0.4	0.3	0.4	30
S27CB-E30NH	3.5	−0.1	−0.1	−0.1	20
V29CG1-A34NH[g]	4.4	0.2	−0.0	0.1	20
V29CG2-A34NH[g]	4.6	0.4	0.4	0.4	20
S27CB-V29NH	3.8	−0.1	−0.2	−0.1	0
V29HA-A34CB[h]	2.4	0.1	−0.0	−0.0	1

[a–d] See Table I for footnotes. [e] In addition, NH(i + 1)–CB(i) (final weights 15 kcal/mol, a pseudoatom correction applied), NH(i)–HA(i), and NH(i)–CB(i) NOEs (final weights 15 kcal/mol) were used starting with the second step of the energy minimization. [f] The weights were set to 300 kcal/mol for the (A) and (M) starts, and 0 kcal/mol for the (L) start. [g] See footnote *e* Table I. The $J_{\alpha\beta}$ coupling constant for Val-29 is 11 Hz. [h] 0.33 Å was subtracted from rather than added to the calculated constraint because other constraints require that HA of V29 is closer to the carbon atom than to the protons of the A34 methyl group.

Examination of the calculated structures shows that residues 29–32 adopt a slightly distorted β-turn type I. The NOE pattern of NH(i)–NH(i + 1) and HA(i)–NH(i + 1) corresponds to that of β-turn type I. However, the expected (i)–(i + 2) and (i)–(i + 3) connectivities E30HA–L32NH, E30NH–L32NH, and V29HA–L32NH are not seen because distances in the final structures (4.3, 4.7, and 4.7 Å, respectively) are larger than those for a perfect β-turn (3.6, 3.8, and 3.1–4.2 Å, respectively) (Wuthrich et al., 1984). The calculated structure is not unknown in proteins. When viewed from another angle than that used in Figure 4, the calculated structures of segment 26–36 are easily recognized as a right-handed loop (Richardson, 1981). This type of a structure frequently precedes an α-helical segment. In ACP, residues 26–36 do precede a known α-helix at residues 37–51 (Holak & Prestegard, 1986).

Thus, the methodology described appears to provide a possible route to structure determination by NMR. One

cannot be assured of total avoidance of local minima nor of identification of a completely unique structure, but in the two cases investigated viable structures, having similar conformations, are produced from very different starting points. The calculations are reasonably efficient as executed here. The longest calculations, those starting from the linear conformation, required approximately 4 h on a VAX 11/750 with a floating-point accelerator. Although direct comparison to calculations on different structures is difficult, this time is likely to be longer than the time required for structure determination of molecules of similar size using distance geometry programs and shorter than that required using molecular dynamics on molecules of comparable size (Clore et al., 1985). Use of a torsionally unconstrained chain, along with a suitable NMR pseudoenergy function to represent limited distance information in early stages of energy minimization, followed by stepwise introduction of other bonding and nonbonding energies appears to help in avoiding local minima. Even when structures representing local energy minima are produced, they are easily identified and discarded.

ACKNOWLEDGMENTS

We thank J. N. Scarsdale for assisting with the computational aspects of the work.

REFERENCES

Anil Kumar, Wagner, G., Ernst, R. R., & Wüthrich, K. (1981) *J. Am. Chem. Soc. 103*, 3654–3658.

Arseniev, A. S., Kondakov, V. I., Maiorov, V. N., & Bystrov, V. F. (1984) *FEBS Lett. 165*, 57–62.

Braun, W., & Gō, N. (1985) *J. Mol. Biol. 186*, 611–626.

Braun, W., Bosch, C., Brown, L. R., Gō, N., & Wüthrich, K. (1981) *Biochim. Biophys. Acta 667*, 377–396.

Braun, W., Wider, G., Lee, K. H., & Wüthrich, K. (1983) *J. Mol. Biol. 169*, 921–948.

Braun, W., Wagner, G., Wörgötter, E., Vašák, M., Kägi, J. H. R., & Wüthrich, K. (1986) *J. Mol. Biol. 187*, 125–129.

Brünger, A. T., Clore, G. M., Gronenborn, A. M., & Karplus, M. (1986) *Proc. Natl. Acad. Sci. U.S.A. 83*, 3801–3805.

Clore, G. M., & Gronenborn, A. M. (1985) *J. Magn. Reson. 61*, 158–164.

Clore, G. M., Gronenborn, A. M., Brünger, A. T., & Karplus, M. (1985) *J. Mol. Biol. 186*, 435–455.

Clore, G. M., Brünger, A. T., Karplus, M., & Gronenborn, A. M. (1986) *J. Mol. Biol. 191*, 523–551.

Dobson, C. M., Olejniczak, E. T., Poulsen, F. M., & Ratcliffe, R. G. (1982) *J. Magn. Reson. 48*, 97–110.

Ferrige, A. G., & Lindon, J. C. (1978) *J. Magn. Reson. 31*, 337–340.

Gelin, B. R., & Karplus, M. (1979) *Biochemistry 18*, 1256–1268.

Havel, T. F., & Wüthrich, K. (1984) *Bull. Math. Biol. 46*, 673–698.

Havel, T. F., & Wüthrich, K. (1985) *J. Mol. Biol. 182*, 281–294.

Havel, T. F., Crippen, G. M., & Kuntz, I. D. (1979) *Biopolymers 18*, 73–81.

Havel, T. F., Kuntz, I. D., & Crippen, G. M. (1983) *Bull. Math. Biol. 45*, 665–720.

Holak, T. A., & Prestegard, J. H. (1986) *Biochemistry 25*, 5766–5774.

IUPAC–IUB Commission on Biochemical Nomenclature (1970) *J. Mol. Biol. 52*, 1–17.

Kaptein, R., Zuiderweg, E. R. P., Scheek, R. M., Boelens, R., & van Gunsteren, W. F. (1985) *J. Mol. Biol. 182*, 179–182.

Kay, L. E., Scarsdale, J. N., Hare, D. R., & Prestegard, J. H. (1986a) *J. Magn. Reson. 68*, 515–525.

Kay, L. E., Holak, T. A., Johnson, B. A., Armitage, I. M., & Prestegard, J. H. (1986b) *J. Am. Chem. Soc. 108*, 4242–4244.

Keepers, J. W., & James, T. L. (1984) *J. Magn. Reson. 57*, 404–426.

Kline, A. D., Braun, W., & Wüthrich, K. (1986) *J. Mol. Biol. 189*, 377–382.

Kuntz, I. D., Crippen, G. M., & Kollman, P. A. (1979) *Biopolymers 18*, 939–957.

Olejniczak, E. T., Dobson, C. M., Karplus, M., & Levy, R. M. (1984a) *J. Am. Chem. Soc. 106*, 1923–1930.

Olejniczak, E. T., Poulsen, F. M., & Dobson, C. M. (1984b) *J. Magn. Reson. 59*, 518–523.

Richardson, J. S. (1981) *Advances in Protein Chemistry 34* (Anfinsen, C. B., Edsall, J. T., & Richards, F. M., Eds.) pp 167–339, Academic, New York.

Scarsdale, J. N., Yu, R. K., & Prestegard, J. H. (1986) *J. Am. Chem. Soc. 108*, 6778–6784.

Scarsdale, J. N., Yu, R. K., & Prestegard, J. H. (1987) *J. Comput. Chem.* (in press).

States, D. J., Haberkorn, R. A., & Ruben, D. J. (1982) *J. Magn. Reson. 48*, 286–292.

Thompson, G. A. (1981) *The Regulation of Membrane Lipid Metabolism*, pp 20–23, 33, CRC, Boca Raton, FL.

Wagner, G., & Wüthrich, K. (1979) *J. Magn. Reson. 33*, 675–680.

Wagner, G., Neuhaus, D., Wörgötter, E., Vašák, M., Kägi, J. H. R., & Wüthrich, K. (1986) *J. Mol. Biol. 187*, 131–135.

Wakil, S. J., Stoops, J. K., Joshi, V. C. (1983) *Annu. Rev. Biochem. 52*, 537–579.

Weiner, P. K., & Kollman, P. A. (1981) *J. Comput. Chem. 2*, 287–303.

Weiner, S. J., Kollman, P. A., Case, D. A., Singh, U. C., Ghio, C., Alagona, G., Profeta, S., Jr., & Weiner, P. K. (1984) *J. Am. Chem. Soc. 106*, 765–784.

Weiner, S. J., Kollman, P. A., Nguyen, D. T., & Case, D. A. (1986) *J. Comput. Chem. 7*, 230–252.

Weiss, G. H., Ferretti, J. A., & Byrd, R. A. (1987) *J. Magn. Reson. 71*, 97–105.

Williamson, M. P., Havel, T. F., & Wüthrich, K. (1985) *J. Mol. Biol. 182*, 295–315.

Wüthrich, K., Billeter, M., & Braun, W. (1983) *J. Mol. Biol. 169*, 949–961.

Wüthrich, K., Billeter, M., & Braun, W. (1984) *J. Mol. Biol. 180*, 715–740.

Zuiderweg, E. R. P., Scheek, R. M., Boelens, R., van Gunsteren, W. F., & Kaptein, R. (1985a) *Biochimie 67*, 707–715.

Zuiderweg, E. R. P., Boelens, R., & Kaptein, R. (1985b) *Biopolymers 24*, 601–611.